Industrial Crops and Products 77 (2015) 691–702

Contents lists available at ScienceDirect

Industrial Crops and Products

journal homepage: www.elsevier.com/locate/indcrop

# Residual sisal fibers treated by methane cold plasma discharge for potential application in cement based material

B.N. Barra [a,*], S.F. Santos [b], P.V.A. Bergo [a], C. Alves Jr. [c], K. Ghavami [d], H. Savastano Jr. [a]

[a] Universidade de São Paulo (USP), Departamento de Engenharia de Biossistemas, Pirassununga, SP, Brazil
[b] Universidade Estadual Paulista (UNESP), Departamento de Materiais e Tecnologia, Guaratinguetá, SP, Brazil
[c] Universidade Federal Rural do Semi-Árido (UFERSA), CiTED—Centro Integrado de Inovação Tecnológica do Semiárido, Mossoró, RN, Brazil
[d] Pontifícia Universidade Católica do Rio de Janeiro (PUC-RJ), Departamento de Engenharia Civil., Rio de Janeiro, RJ, Brazil

ARTICLE INFO

*Article history:*
Received 20 May 2014
Received in revised form 16 June 2015
Accepted 26 July 2015
Available online 3 October 2015

*Keywords:*
Capacitance
Dielectric constant
Contact angle
Lignocelulosic fibers
Portland cement

ABSTRACT

The use of residual sisal fiber is becoming more frequent as reinforcement element in organic or inorganic matrix due to its low cost, high abundance in some countries and constitutes a renewable material. However, a significant loss in the mechanical performance in long term has been observed in fiber-cement composites after natural aging. These alternative fibers can be utilized in a hybrid fiber-cement in order to decrease the content of traditionally used synthetic fibers. The objective of this work was to evaluate the potential of the methane cold plasma treatment of 10 min duration on structural and physical properties of the residual sisal fibers to mitigate the degradation mechanisms when applied to cementitious matrices. Moisture sensitivity evaluation by capacitance method, dielectric measurements, X-ray diffraction, Fourier transform infrared (FTIR), spectroscopy, scanning electron microscopy (SEM), energy dispersive X-ray spectroscopy (EDS), atomic force microscopy (AFM), angle contact and pullout test were carried out in order to follow the effect of the proposed treatment. Besides, mechanical behavior of untreated and treated sisal fibers was evaluated before and after accelerated aging in cementitious solution at 60 °C by 72 h. The results obtained in all these tests confirmed the high potential of the methane cold plasma treatment to delay the degradation of the residual sisal fibers in the presence of a Portland cement environment and these fibers present the higher pullout load and shear stress than one untreated.



## 1. Introduction

In the past decades, related issues to environment and social development have been the challenge of different fields of the industry, as well as, the theme of several studies around the world. Thus, the construction industry, known for being an emergent sector with significant participation in the economy of developed and undeveloped countries, have to incorporate the sustainability in its production process, since the sector has as drawback the massive use of the natural resources (both renewable and non-renewable), waste generation and a high energy consumption (Ortiz et al., 2009; Pacheco-Torgal and Jalali, 2011). One way to minimize this backdrop is the replacement of the fossil fuel based fibers by vegetable fibers as reinforcement in products such as flat or corrugated roofing materials, water containers and cladding panels (Tonoli et al., 2013).

### 1.1. Sisal fiber

Lignocellulosic fibers have reached a remarkable importance as high specific strength materials, for a broad use in the composite materials. In view of the significant advantages provided by the lignocellulosic fibers, mainly due to low-cost production and large availability in nature, there is an increase in the potential use of these fibers in civil engineering (Pereira et al., 2013; Mármol et al., 2013). Moreover, the vegetable fibers come from renewable, have low density, and they are obtained with low energy consumption. Additionally, the creation of this new market could benefit the economy of the producing regions that are generally connected to products of low added value, such as cordage and packing industry. Tropical countries such as Brazil have an abundance of crops for fiber suppliers, many of which are located in underdeveloped or developing regions. The diversity of plants that can provide fiber generates numerous possibilities for production and application, such as sisal (*Agave sisalana*), which is easily available and can be produced even under arid climate conditions (Li et al., 2000). Further, the partial replacement of synthetic fibers (e.g.polypropylene,

* Corresponding author.
*E-mail address:* bruna.barra@usp.br (B.N. Barra).

http://dx.doi.org/10.1016/j.indcrop.2015.07.052
0926-6690/

glass and polyvinyl alcohol) by sisal fibers as a reinforcement element has been of advantage for the fabrication of composite materials in the last years (Tonoli et al., 2011; Tan et al., 2012).

The use of sisal fiber is becoming more frequent, for example, in the toughening of cementitious composites (Gutiérrez et al., 2005; Tan et al., 2012). Besides, some residual sisal fibers commonly sold to the paper and matting industry, such as wadding, crude or cleaned, and also waste brushed or unbrushed, can be utilized for these purposes (Bledzki and Gassan, 1999; Satyanarayana et al., 2007).

However, significant losses in the mechanical performance in long term have been observed in sisal fiber-cement composites after natural or accelerated aging, due to the degradation mechanisms of the cellulose fibers in the cementitious environment (Toledo Filho et al., 2000; Savastano Jr. et al., 2005, 2009; Silva et al., 2011; Melo Filho et al., 2013). The degradation of the vegetable fiber is caused by the alkaline environment with pH > 12 (Toledo Filho et al., 2000). Some progressive degradation mechanisms may take place, such as the destruction of macromolecular chains during the partial alkaline hydrolysis of the cellulose, which causes their rupture and the consequent decrease in the degree of polymerization. This degradation occurs by the easy movement from the pore water towards the surface of the fibers. Another mechanism is the gradual filling of the inner cores of the vegetable fibers with the hydration products leading to the embrittlement of the fibers, reducing their mechanical performance (Melo Filho et al., 2013; Silva et al., 2011; Pavasars et al., 2003; Scrivener and Young, 1997). These mechanisms could affect some important physical properties of the material reinforced, such as adhesion toughness mechanisms and, consequently, mechanical properties (Bentur and Mindess, 2007). The volume stability of the fiber in a water based environment is also crucial in the conservation of the fiber-matrix adhesion Tonoli et al., 2009).

### 1.2. Methane cold plasma

The deposition of hydrophobic coatings on the surface of the fiber counteracts some degradation mechanisms such as the deposition of calcium hydroxide crystals in the interior of the fiber and the attack of other ions from cement suspension on the fiber surface. Recently some applications of plasma-based techniques to coating processes have made a significant progress to improve surface characteristics of the fiber materials (Kim et al., 2006). The surface treatment with cold plasma has been applied in the study of adhesion between several kinds of polymers or biopolymers through the modification of the surface free energy for efficient functionalizing (Mahlberg et al., 1998; Novak et al., 2008). The cold plasma treatment is a useful technique that utilizes ionized gas, at negative pressure, composed by a mixture of neutral species (atoms, molecules and free radicals), electrically charged species (electrons, positive and negative ions), photons, radicals, and excited molecules produced by electric discharge (Wielen and Ragauskas, 2004; Wielen et al., 2006; Gaiolas et al., 2008, 2009; Kalia et al., 2011; Costa et al., 2006). Although the surface property alterations obtained with cold plasma treatment are very complex, they offer an efficient and reliable mechanism to alter surface properties of materials without affecting the bulk properties of the treated substrate (Carlsson and Ström, 1991; Rolf and Sparavigna, 2010). For example, plasma species do not penetrate deeper than about $100 \times 10^{-10}$ m from the surface which means that more than 99% of the bulk of a 10 μm thickness polypropylene film remains unchanged (Hua et al., 1997). The most important factor is that the substrate surface properties change significantly after a few minutes of plasma treatment. Plasma treatment of chemithermomechanical pulp resulted, as in the case of the pulp, in an increment in the quantity of tagged functionalities, which was seen mainly for

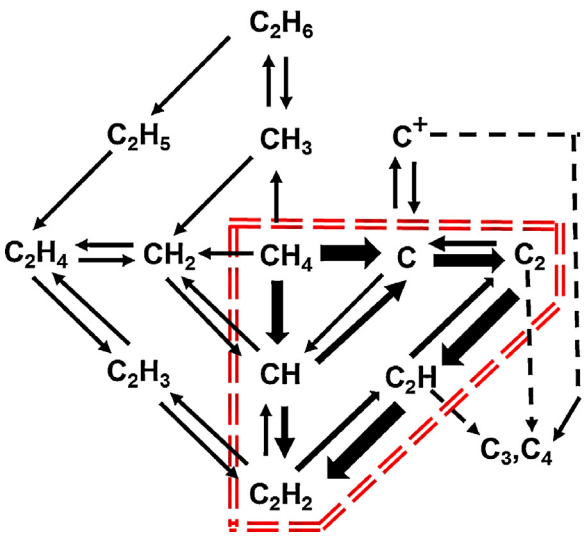


**Fig. 1.** Schematic diagram of the methane gas fragmentation of the methane gas produced in the cold plasma system.
Adapted from Kado et al.(2003).

carboxyl and carbonyl groups (Östenson et al., 2006). This has significant implications for the lignocellulosic fiber industry (Olaru et al., 2005; Wielen et al., 2005; Kalia et al., 2011; Anwer and Bhuiyan, 2012). Due to the physical process the treatment does not make use of water and chemicals and thus is considered quick and environmentally friendly without generating any contamination. Besides the operating costs are lower than some chemical treatments, such as those based on silanes (Shenton and Stevens, 2001; Indarto et al., 2005; Morent et al., 2008; Felekoglu et al., 2009; Navarro et al., 2009).

Based on the outcomes of interactions with materials, cold plasmas can be classified into the broad categories like as plasma polymerization, plasma treatment, and plasma etching (Siow et al., 2006). When cold plasma is generated from a pure organic gas (e.g., methane) or mixed with other gases, a collision occurs between energetic electrons and gas molecules resulting in the formation of a series of reactive fragments, which are recombined to give rise to a solid polymeric material which is deposited on the surface to be treated, or just some functional groups can be grafted on the surface (Kim et al., 2006; Bozaci et al., 2013). This process is known as plasma polymerization. The plasma contains a variety of species including electrons with energies great enough to break molecular bonds from organic gas by collision (Kumar et al., 2010).

Fig. 1 shows a schematic diagram of possible fragments produced in the methane cold plasma for non-equilibrium (non-thermal) discharge. The highlighted region indicates the compound most likely to occur. The thickness of the arrows is correlated to the most probable reactions to occur, as well as, dash line arrows are related to lower probability reactions. Although the dehydrogenation of $C_2H_6$ rapidly produces $C_2H_4$ and $C_2H_2$, the contribution of that reaction path is small because the composition of $C_2H_6$ in the discharge region is very low due to the low $CH_3$ concentrations as highlighted in Fig. 1 (Kado et al., 2003). It is accepted that in non-thermal plasma systems, the formation of free radicals and ion-radicals is the decisive stage for the consecutive transformations of methane (Ghorbanzadeh et al., 2005).

### 1.3. Lignocellulosic fiber and methane cold plasma

Based on many XPS studies, the vegetable fiber surface has a series of functional groups that rise up, mainly, from lignin and extractives (C—C, C—H, C=O, O—C—O, COOH, COOC), as well as, from

cellulose and hemicellulose (C—O, C—OH) (Hua et al., 1997; Sain, 2000; Sain and Panthapulakkal, 2006; Sahin, 2007; Popescu et al., 2009; Popescu et al., 2011; Tran et al., 2011; Fuentes et al., 2011). The methane cold plasma discharge induces a series of reactions on the fiber surface, including the formation of hydrophobic alkane radicals ($CH_3$, $CH_2$ and CH) as the result of the interactions with the saturated carbon (C—C, C—H), hydroxyl carbons (C—OH), carbonyl and carboxyl groups.

Simultaneous processes of etching, deposition, degradation, recombination and crosslinking take place on the surface of materials that are plasma treated (Östenson et al., 2006). These interactions could be responsible for the polymerization of the fiber surface, because of the deposition of a thin film of carbon with hydrophobic characteristics (Wielen et al., 2005; Kalia et al., 2011). Sinha and Panigrahi (2009) proposed that there are two major types of reactions possible with cold plasma on fiber surface: (1) surface modification of polymer and (2) polymerizations of the monomers. Thus, with methane cold plasma reactions the characteristics of the lignocellulosic fiber surface such as wettability, adhesive bonding, hydrophilic and hydrophobic tendency are improved (Sadova and Pankratova, 2009).

In this work the potential use of the methane cold plasma treatment to mitigate degradation mechanisms of residual sisal fibers in fiber-cement were analyzed. Additionally, the mechanical behavior of untreated and treated sisal fibers was assessed before and after accelerated aging tests.

## 2. Materials and methods

### 2.1. Materials

The residual sisal fibers used are waste of the baler twine, donated by the Associação de Desenvolvimento Sustentável da Região Sisaleira (APAEB-Valente), located in Bahia (one of the northeast Brazilian states), which were tested without any previous conditioning or treatment.

### 2.2. Plasma treatment

The residual sisal fibers were treated in cold plasma reactor vacuum (Fig. 2a), constituted by a cylindrical tube of borosilicate glass with an outer diameter of 180 mm, an outer height of 300 mm, a capacity of about 7.6 L and two stainless steel flanges (Fig. 2b). The cold plasma treatment with methane gas was generated by direct electric current during 10 min with a gas flow of 5 $cm^3$/min, a distance between cathode and support fibers equal to 70 mm, pressure $6.5 \times 10^{-4}$ MPa; approximately 450 V and electric current of 0.10 A.

### 2.3. X-ray diffraction measurements

For the X-ray diffraction measurements, the residual sisal fibers were cut in small pieces and fixed in a small plate with inert paste, in order to interact with the beam. The X-ray diffraction patterns were

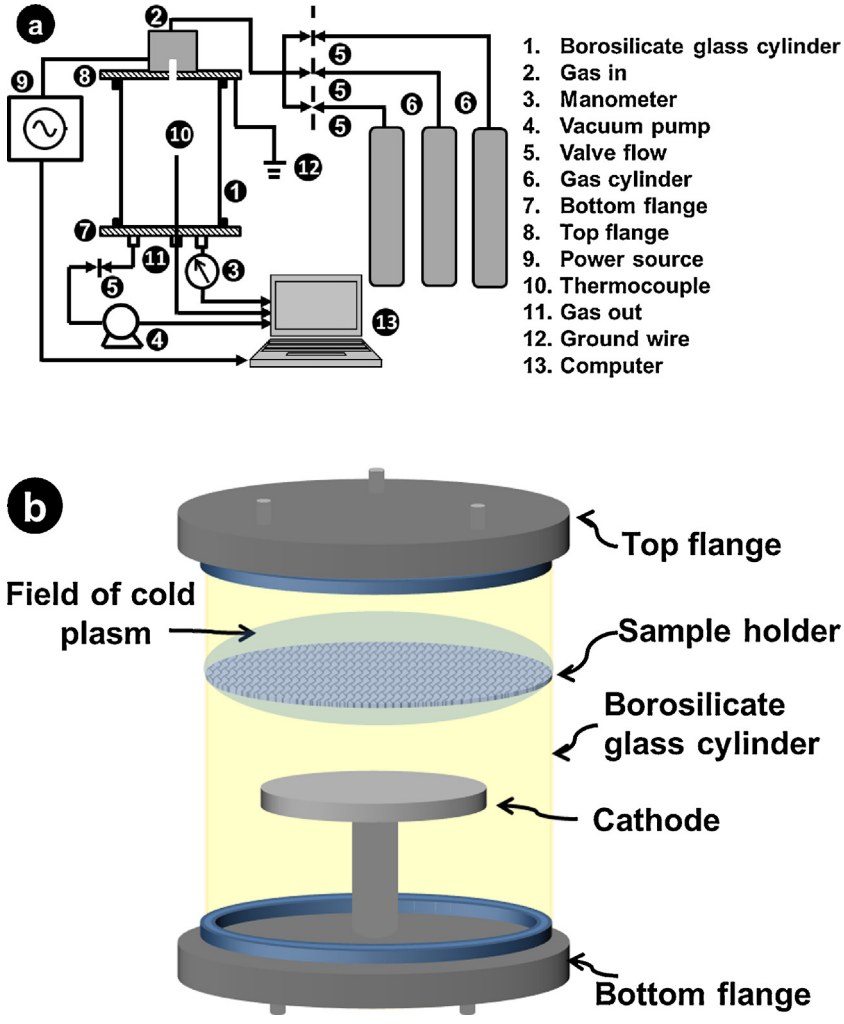


**Fig. 2.** (a) Schematic representation of the cold plasma reactor vacuum; (b) details of the borosilicate glass cylinder. Adapted from Costa et al. (2006).

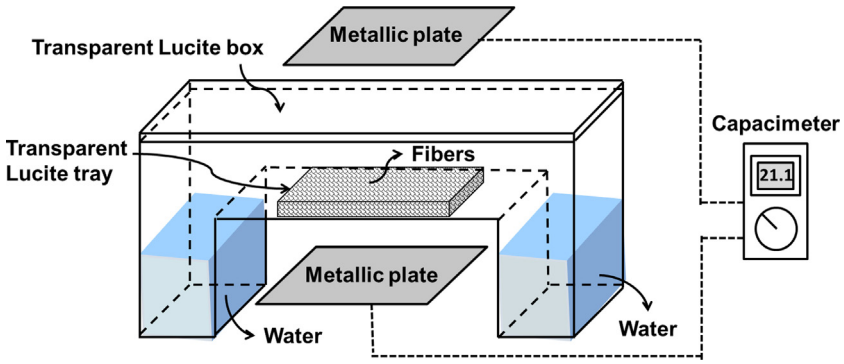


**Fig. 3.** Schematic drawing representing the capacitance method to evaluate the dielectric properties of sisal fibers as function of the amount of moisture adsorbed.

obtained by the X-ray generator theta–theta from diffractometer RIGAKU (Japan) Rotaflex model Ru-200B operating at 40 kV, 20 mA, and with cooper tube, $\lambda$(Cu K$\alpha$) = 1.5406 Å, at room temperature. The beam angle ($2\theta$) varied from 10 to 30°.

### 2.4. Infrared spectroscopy

FTIR spectroscopy is a nondestructive method for studying the physic-chemical properties of a bulk material. Infrared spectra (FTIR) of the fibers were recorded between 4000 and 600 $cm^{-1}$ at 2 $cm^{-1}$ of resolution, with a Spectrum One (PerkinElmer) spectrometer, supplied with a universal attenuated total reflectance (UATR) accessory. For each spectrum, 26 scans were co-added. A small amount of fibers was carefully placed over the cell and pressed conveniently in order to maintain the same pressure, for reflectance operation mode. Measurements were performed at room temperature.

### 2.5. Moisture adsorption

Sorption is most often described as a common term when thinking of the phenomena adsorption (gain of moisture from the surrounding air) and desorption (loss of moisture to the surrounding air). In this work the moisture gain in sisal fibers was evaluated at different periods, for untreated and treated fibers by methane cold plasma discharge (10 min). For this test, the fiber samples were dried in a stove (Marconi, model MA035, Brazil) with forced air circulation at 60 °C for a period of 1 h, then weighed in an analytic scale Mod. Marte (USA). After this the samples were conditioned at 98% relative humidity and 25 ± 2 °C at different periods until the establishment of the equilibrium. For periods beyond 8 days, the moisture content was found to attain the equilibrium for all samples. The moisture content ($X$) is expressed always on the basis of dry solids ($X$ = g water/g dry solids). Measurements were performed in duplicate.

### 2.6. Capacitance method

Dielectric property is the ability of electrical dipoles in an insulator to polarize under an external electric field. Materials that possess electric dipoles including water molecules exhibit considerable dielectric properties. Therefore the dielectric constant (and thus, capacitance) of wet and dry materials changes considerably according to the amount of moisture adsorbed. For capacitance measurements, a capacimeter mod. Instrutherm CP-400 (USA) was used. This instrument applies an alternating electric field near 800 Hz on the capacitance probe (metallic plates). Fig. 3 shows details and dimensions of the setup used in these experiments and performed at room temperature. The cell (sample holder) was made with a transparent Lucite box, assembled in an inverted "U" shape, with the two rigid and parallel metallic (aluminum) plates mounted as shown in Fig. 3, forming a capacitor. Small amounts of fiber samples were carefully compacted inside small trays made of transparent Lucite. This tray was placed inside the Lucite box, in the region between the metallic plates, for measuring the capacitance. For relative humidity (RH) control inside the box, water was used, as shown in the figure, in order to simulate an environment with 100% RH. Before measurements were taken, the fibers were dried in a stove (Marconi, model MA035, Brazil) with forced air circulation by 60 °C for a period of 2 h in order to remove any trace of moisture content. After this step, the capacitance measurements were taken during the exposure of the fibers inside the Lucite box until the establishment of the equilibrium. The response was the capacitance variations during the exposure time of the fibers at this simulated environment.

### 2.7. Contact angle goniometer

The surface energy can be obtained indirectly through the contact angle of a pure liquid droplet on the solid substrate by means of the sessile drop method. The static water contact angle ($\theta$) after about 10 s of dropping deionized water at 25 ± 2 °C was measured by Krüss Easy Drop goniometer (Krüss, GmbH, Hamburg–Germany) equipped with a digital photo analyzer using the sessile drop technique to observe surface characteristics of the residual sisal fiber before and after methane cold plasma treatment. Multiple droplets of 0.22–0.30 μL were deposited in several places throughout on the single fiber to determine possible heterogeneity, and the average of five fibers was used to calculate each $\theta$. The analysis of variance (ANOVA) followed by Tukey test were applied to compare the mean results between groups at a significance level of 5%.

### 2.8. SPM imaging analysis

The surface morphology of the residual sisal fiber before and after methane cold plasma discharge was analyzed using a Scanning Probe Microscope (SPM) (NT-MDT, Moscow, Russia), Solver Next. Images were acquired in contact mode in air using tetrahedral tip model N-type Si cantilever with a reflective side of gold and a radius between 6 nm and 10 nm. Force curves were measured at the nominal resonance frequency of 1 Hz and a spring constant of the cantilever of 0.03 N/m.

### 2.9. Accelerated aging

In order to assess the effect of the methane cold plasma treatment in the residual sisal fiber an accelerated aging test was carried out based on methodology proposed by Ramakrishna and Sundararajan (2005). The sisal fibers of 8 cm length (untreated and treated one) were kept immersed in a borosilicate glass boiling

**Table 1**
Chemical composition of the ordinary Portland cement CP V-ARI.[a]

| Compounds | $SiO_2$ | $Al_2O_3$ | $Fe_2O_3$ | CaO | MgO | $SO_3$ | $K_2O$ | $Na_2O$ | L.O.I.[b] |
|---|---|---|---|---|---|---|---|---|---|
| Content (%wt) | 20.14 | 4.94 | 3.07 | 62.87 | 1.39 | 3.4 | 0.95 | 0.15 | 2.22 |

[a] Brazilian Standard NBR 5733 (clinker + gypsum = 100 – 95% by weight; calcium carbonate filler = 0–5%)
[b] L.O.I.: Loss on ignition

flask with three short necks. The accelerated aging test was carried out for 72 h in saturated ordinary Portland cement solution with deionized water at 60 ± 1 °C, controlled by a hot plate and temperature sensor system. After this time the fibers were kept in a stove (Marconi, model MA035, Brazil) with a forced air circulation by 60 °C/24 h and the ultimate tensile strength was determined. During the period of exposure, the pH of the solution was maintained between 11 and 12 with the use of a pH meter (DM-23, DME-CV1 model, Digimed, Brazil). The carbonation of the ordinary Portland cement solution was avoided by sealing the necks of glass boiling flask. The Brazilian ordinary Portland cement, type CP V-ARI (high initial resistance, Table 1) was utilized in this work. The use of this cement is justified because it is commercially available, without pozzolanic or blast furnace slag additions and has a lower content of limestone filler.

### 2.10. Scanning electrons microscope

The residual sisal fibers were examined by scanning electron microscope (SEM) in backscattered electron mode using Hitachi Analytical Table Top Microscope TM 3000 and the environmental scanning electron microscope (ESEM) in backscattered electron mode and energy dispersive X-ray spectroscopy (EDS) using FEI quanta 600, before and after accelerated aging test.

### 2.11. Mechanical properties

The tensile strength of the residual sisal fiber was determined using a single residual sisal fiber in an universal testing machine EMIC DL 30000 with a displacement speed of 0.4 mm/s. Fifteen fibers were tested. The transversal section of the fibers was obtained by an optical microscopy Zeiss, model AxioImager.A2m and a digital camera model Axiocam MRc5 (German). According to the observations, it was found that the cross section area of the sisal fibers is variable and its geometry is roughly elliptical along the length. For this reason, a correction factor was determined between the actual area and the elliptical area which is calculated from the major and minor axes of the fiber cross section. Besides, the real area was considered, corrected by a correction factor for each fiber tested (Motta et al., 2010). The fiber was conveniently fixed in the paper mask apparatus, according to the scheme of Fig. 4, in the attempt to avoid tension concentration or eccentricity during the development of the test.

### 2.12. Pullout test

For the pullout test cement paste cylinders were molded with a single fiber centrally aligned with an embedded length of 25 mm, in accordance with the methodology used by Ferreira et al. (2012). The matrix composed of filler, binders (30% Portland cement, 30% metakaolin, 40% fly ash) and water. The cylinder specimens remained in the mold for 24 h and after demolding were kept in a humid chamber for 7 days to cure. After curing, the specimens remained for one day under 23 °C ± 1 °C temperature and relative humidity of 43% ± 3% for removal of excess water present in the fiber. After drying the specimens were tested in electromechanical universal testing machine, Shimadzu, AGS-X, with a load cell of 1 kN and displacement rate of 0.1 mm/min.

From the pullout test, it was calculated the shear stress, $\tau$, between fiber and matrix using the following equation:

$$\tau = \frac{P}{2\pi r L} \quad (1)$$

where $P$ is load, $L$ is embedded length of the fiber and $r$ is the fiber radius obtained by scanning electron microscopy.

## 3. Results and discussions

### 3.1. SEM analysis

Fig. 5 shows the untreated surface of a residual sisal fiber with the deposition of calcium oxalate microplates. Many vegetable fibers accumulate calcium oxalate as it has been reported in different vegetable species. The calcium oxalate crystals can occur in a wide range of morphologies. These morphologies include block-like prismatic crystals, present as single or multiple crystals, with large elongated rectangular shapes (Franceschi and Nakata, 2005). They are highly insoluble and dissolve poorly in water. However, in the sisal fiber there is not a large enough quantity of calcium oxalates to be detected by the ordinary X-ray diffractometer method.

The SEM images of untreated and treated sisal fibers after accelerated aging are shown in Fig. 6. The cement solution produced some compounds such as $SiO^2(H_2O)x$, $K^+$, $Na^+$, $SO_4^{2-}$, $Al^{3+}$ and $OH^-$ ions that were highly effective at binding the calcium ions (Taylor, 1997) and thereby decreasing the concentration of calcium in solution, shifting the reaction equilibrium so that more calcium oxalate of the sisal fiber can be dissolved.

Although both, untreated and treated, surface sisal fibers had been attacked by ions in the interval of three days in the saturated

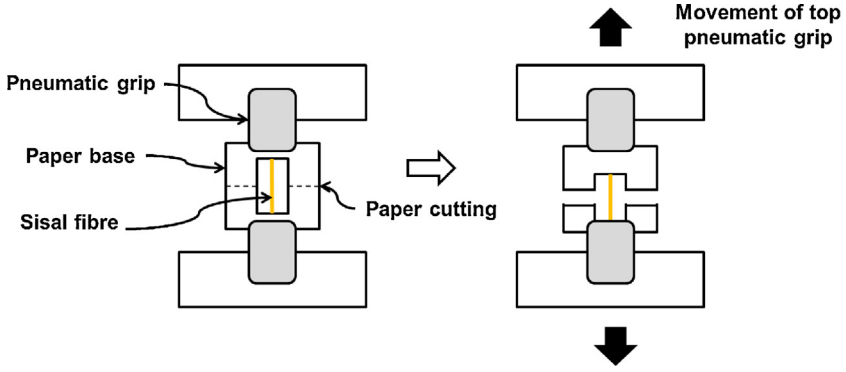


**Fig. 4.** Schematic representation of the mechanical tests of the sisal fibers.

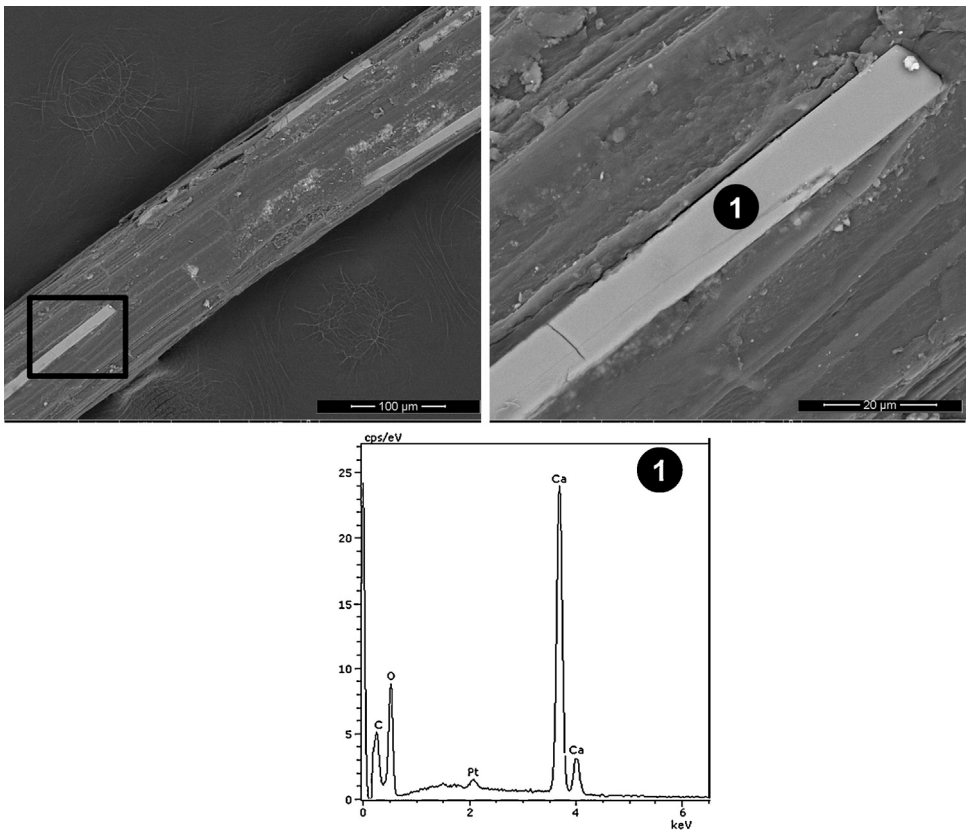


**Fig. 5.** SEM images in backscattered electron mode of untreated surface sisal fiber with respective detail of calcium oxalate microplate. The number "1" indicates the point of the energy dispersive X-ray spectrum.

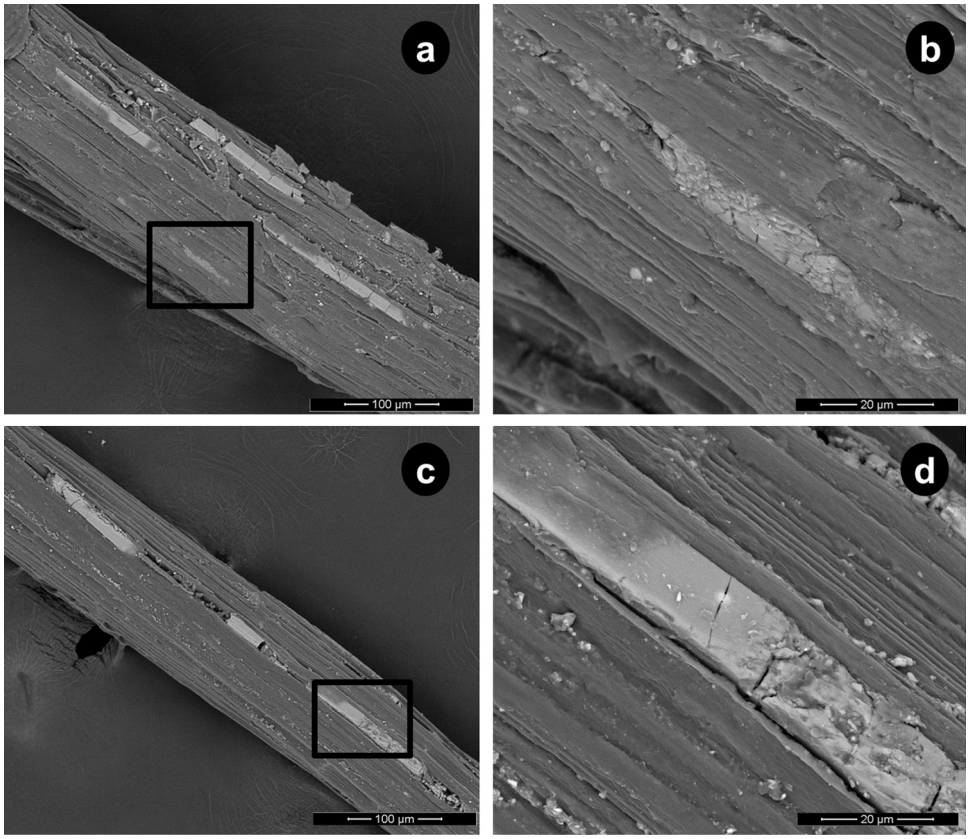


**Fig. 6.** SEM images in backscattered electron mode of surface sisal fiber after accelerated aging with respective amplified images showing details of deteriorated calcium oxalate microplates and surfaces. Untreated (a) and (b), and treated sisal fibers (c) and (d).

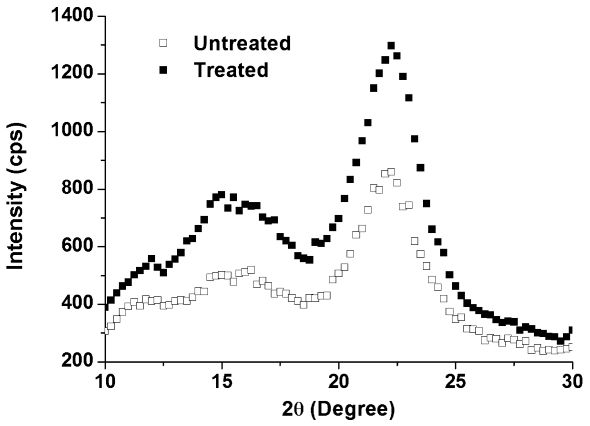


**Fig. 7.** X-ray diffraction pattern of untreated and treated sisal fibers.

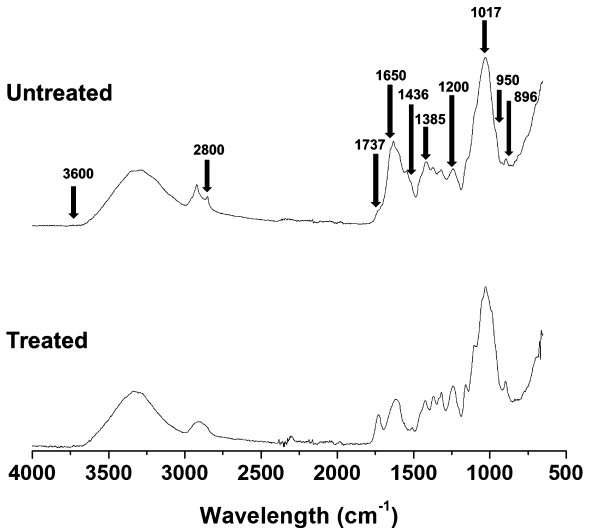


**Fig. 8.** FTIR spectra of the untreated and treated sisal fibers.

cement solution at 60 °C there is a significant difference between their surface structures.

### 3.2. X-ray diffractions patterns

The structure of sisal fibers is complex, and in that it comprises different hierarchical microstructures. This is basically due to the composite-like structure of lignocellulosic fibers that are mainly made up of a complex network of three biopolymers: cellulose (semi crystalline), hemicellulose (amorphous) and the lignin (aromatic polymer) (Satyanarayana et al., 2007; Moniruzzaman and Ono, 2013). The X-ray diffraction patterns depicted in Fig. 7 show three peaks at 2$\theta$ (degree) equal to 14.76°, 16.44° and 22.56° confirmed that mainly native cellulose is present (Liu and Hu, 2008). These peaks are also related to the semi crystalline main fraction of the cellulose microfibril. The amorphous fraction is associated to region from 2$\theta$ value of 10–20°. Thus, according to the X-ray diffraction patterns, the sisal fiber bulk was not apparently changed by methane cold plasma treatment. The fiber is assembled by gluing together a bundle of very small fibers called fibril. The glue holding the fibrils together is lignin. Fibrils are made up of microfibrils which in turn are made up of cellulose and hemicellulose polymers. The cellulose microfibril can be considered as a single thin and long crystalline and amorphous entity with highly anisotropic physical properties (Nishiyama, 2009). The free hydroxyl groups present in the cellulose macromolecules are likely to be involved in a number of intramolecular and intermolecular hydrogen bonds, which may give rise to various ordered crystalline arrangements. In the case of cellulose and its derivatives, these crystalline arrangements are usually imperfect (Pérez and Mazeau, 2005).

### 3.3. FTIR results

The FTIR spectra of untreated and treated sisal fibers are shown in Fig. 8. The dominant peaks in the region between 3600 and 2800 $cm^{-1}$ are due to stretching vibrations of OH and CH, respectively. The prominent peaks between 1737 $cm^{-1}$ in the sisal fiber are attributed to either the acetyl and uronic ester groups of the hemicelluloses or the ester linkage of carboxylic group of the ferulic and *p*-coumeric acids of lignin and/or hemicelluloses. The absorption at 1650 $cm^{-1}$ is principally associated with absorbed water in crystalline cellulose (Sinha and Panigrahi, 2009; Kačuráková et al., 1998). The region from 1436 $cm^{-1}$ to 1385 $cm^{-1}$ represents the aromatic C=C stretch of aromatic rings of lignin and the peaks can reflect C—H asymmetric deformations. The peaks in the region 1200–950 $cm^{-1}$ are due to C—O stretching. The peak near 1017 $cm^{-1}$ is assigned to strong hydrogen bond or C—O—H vibrations. The increase of the band at 896 $cm^{-1}$ indicates the typical structure of cellulose (Alemdar and Sain, 2008; Alvarez and Vázquez, 2006). The FTIR technique showed also that there are no significant differences between untreated and treated sisal fibers in the peaks near 2800 $cm^{-1}$ and 1737 $cm^{-1}$. At 2800 $cm^{-1}$ two weak peaks merged and at 1737 $cm^{-1}$ a new peak appeared after methane cold plasma treatment indicating some chemical modifications.

### 3.4. Surface topography

The surface morphology of the untreated and treated fiber surfaces derived from SPM in contact mode are shown in Fig. 9. These images detail the rough primary wall and middle lamella which is characteristic of fibers. However, it is difficult to make a distinction between the two layers. The middle lamella is very thin and composed of 70% lignin associated with a small amount of hemicellulose, cellulose and pectin, which binds the microfibrils. Therefore, they are often referred to as composed lamella. (Xu, 2010; Gandini and Belgacem, 2008). The treatment affected the surface roughness of the fibers. The root-mean-square surface roughness (measured for 4.0 μm × 4.0 μm) was measured. The untreated fiber presented a root mean square roughness, RMS, of about 59 nm and treated fiber about 37 nm. Kim et al. (2006) have reported that the $CH_4$ plasma polymerization deposited a very smooth hydrocarbon layer exposing —$CH_2$ and —$CH_3$ groups leading to increased hydrophobicity.

### 3.5. Moisture content

Fig. 10 shows the moisture content of untreated and treated sisal fibers when exposed to 98% relative humidity and 25 ± 2 °C at different periods until the establishment of the equilibrium. The sisal fiber contains about 74–75.2 wt% of α-cellulose, 10–13.9 wt% of hemicellulose and 7.6–8 wt% of lignin (Satyanarayana et al., 2007). The hemicellulose is a branched polysaccharide composed mainly of pentosanes and hexosanes, which contain a large number of hydroxyl groups. Because of its branched formation and complex chemical structure, its contribution to the polar behavior is higher than cellulose. Finally, lignin is an aromatic polymer with a high content of branched molecules (Rangel-Vázquez and Leal-García, 2010). The hydrophobic nature of the lignin on the other hand acts as a cementing agent and increases the stiffness of the cellulose/hemicellulose composite. Therefore, the lignin is a waterproof material, enabling the transport of water and solutes through

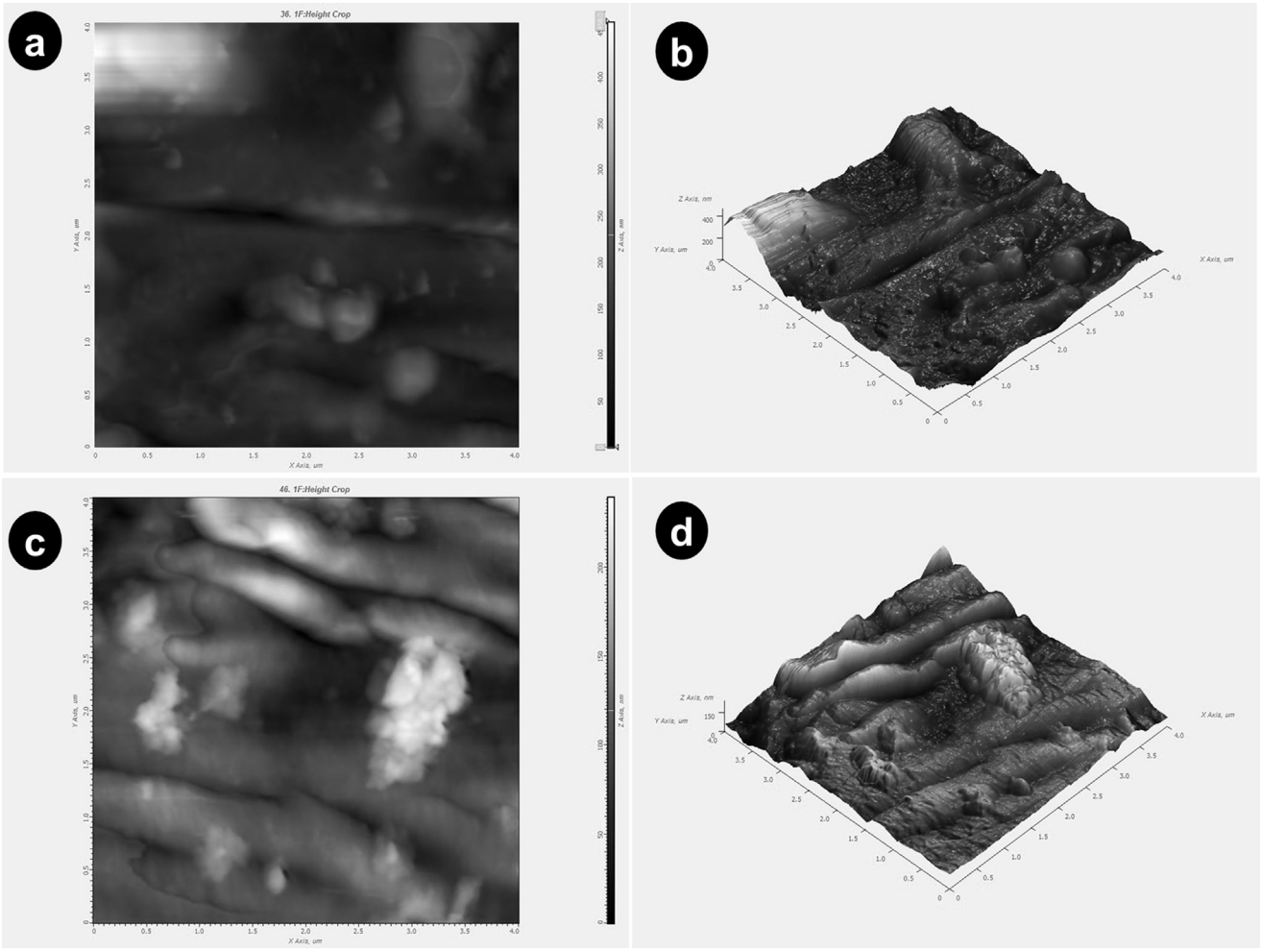


**Fig. 9.** Morphology of fiber surfaces obtained from deflection SPM image data. SPM images in 2D and 3D, respectively, before (a) and (b) and after (c) and (d) methane cold plasma treatment.

the vascular system, and plays a role in protecting plants against pathogens (Boerjan et al., 2003; Thomas et al., 2011). Therefore, according to the results, the untreated fibers presented more the inherent polar and hygroscopic nature of the celluloses given by the greater amount of water absorbed. In treated fibers by the methane cold plasma, the water absorbed amount is smaller than in the untreated fibers. Thus, the treatment of 10 min provided enough modification in the surface and electrical properties of the residual sisal fiber. This behavior was also found in another work, including samples of cellulosic fibers treated by dielectric barrier discharge (Wielen et al., 2006). Functional groups and cross-links are introduced at the fiber surface by reaction among gas-phase species and surface species. Plasma polymerization involves the fragmentation and subsequent deposition of hydrophobic organic monomers that can delay adsorbed water in the fiber (Siow et al., 2006; Friedrich, 2011).

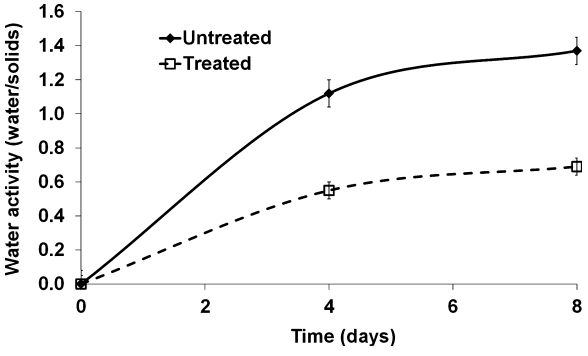


**Fig. 10.** Moisture content of the untreated and treated sisal fibers.

At surfaces of fiber, water can be adsorbed at three levels: monolayer-adsorbed moisture, adsorbed moisture and condensed moisture. Adsorbed water molecules are affected by influencing van der Waals interactions, as well as the ratio of the binding to diffusion forces for water molecules on the solid surface. The initially adsorbed water molecules in high energy sorption centers in the solid surface can form a monomolecular layer. As more water molecules adsorb onto the surface fiber, they are subjected to surface binding and the diffusion forces induce water to penetrate into the fiber through the microporous. Simultaneously, condensed moisture like gel is formed onto monolayer. And finally, the water can enter in multilayer and free water domain at the fiber surface and lumens.

### 3.6. Capacitance measurements

Fig. 11 illustrates the dielectric response of the fiber samples subjected to a 100% relative humidity atmosphere. The capacitance increased with the increasing of the water adsorption until the establishment of the equilibrium (moisture saturation in the fiber) for both types of fiber (Fig. 11). The time elapsed to untreated

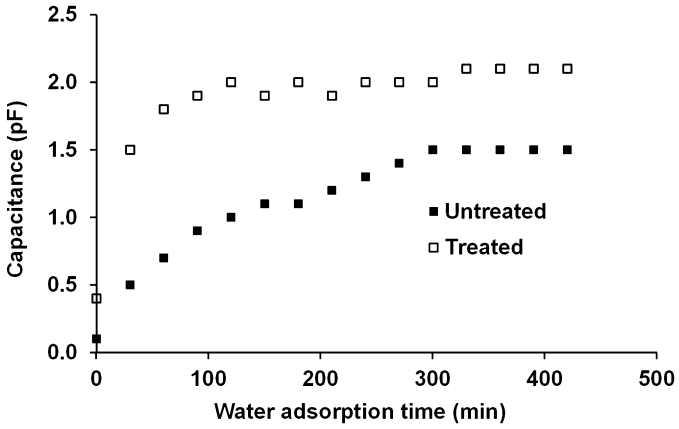


**Fig. 11.** The capacitance characteristics of the untreated and treated sisal fibers as a function of water adsorption time.

**Table 2**
Dielectric constant values of sisal fibers before and after treatment with discharge plasma.

| Condition | Untreated | Treated |
|---|---|---|
| Dielectric Constant value | 1.5 ± 0.3 | 3.1 ± 0.3 |

fibers to attain the equilibrium can be estimated to be near 300 min and for treated fibers near 200 min, which means that the hygroscopic nature of fibers was affected by the methane cold plasma treatment. The variations of the capacitance with water content in cellulosic fiber can be explained by the way the water molecule interacts with the biopolymer by the chemical and physical adsorptions of water molecules existing in the studied atmosphere. As moisture increases, an additional layer of water molecules begin to be formed, over an already formed chemisorbed layer (monolayer). Also it was observed that as moisture increases on the surface of sisal fiber a great number of physical adsorption layers are formed, which in turn markedly affects the measured capacitance, as can be seen by the results depicted in Fig. 11 (Mahadeva et al., 2011). Therefore, the hydrophilic groups like C–O and C–OH, were affected after treatment.

The cold plasma using methane gas ($CH_4$) can be causing the surface polymerization, providing the formation of hydrophobic dipolar alkane radicals ($CH_3$, $CH_2$ and CH), which could explain the highest dielectric constant (Table 2).

There is a collective effect of induced dipoles (contributions from bond water and hydrophobic dipolar alkane radicals) on the capacitance of the treated fiber surface. In molecules located at the surface, the dipole moment results from the fact that there is a specific distribution of positive and negative charges. In fact, the dipole moment of a molecule is determined by integration over the charge distributions on the surface. The deposition of hydrophobic organic monomers (free radicals hydrophobic groups) contributed strongly to increase the dielectric constant in the first stage of hydration of the treated fiber.

### 3.7. Contact angle measurements

The surface energy of the fiber is closely related to the hydrophobicity, and hence with the contact angle between a liquid and fiber surface. The increase of the contact angle with the water means hydrophobization of the fiber surface. Fig. 12 shows the effect of the methane cold plasma treatment on the surface energy of the residual sisal fibers. The treatment significantly increased the contact angle of the sisal fiber (Table 3). A higher contact angle indicates a higher difficulty in forming a water monolayer on the fiber

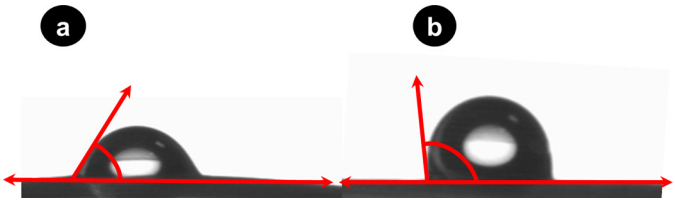


**Fig. 12.** Images of water droplets on surface fibers with contact angle representations. (a) Untreated and (b) treated fibers.

**Table 3**
Contact angle values of sisal fibers.*

| Condition | Untreated | Treated |
|---|---|---|
| Contact angle (degree) | $83^\circ \pm 13^{\circ a}$ | $105^\circ \pm 4^{\circ b}$ |

* Columns with means followed by different letters differ by Tukey test at 5% probability ($P < 0.05$).

surface, as well as adsorption of water is retarded. Thus, this result corroborated to moisture measurements as shown, previously, in Fig. 12.

### 3.8. Ultimate tensile strength distribution

The ultimate tensile strength values of the residual sisal fibers varied between 129 MPa and 378 MPa before accelerated aging, according to the distribution showed in Fig. 13a. These results indicate that the residual fibers are weaker than non-residual sisal mentioned in the literature, where the ultimate tensile strength values vary between 324 MPa and 577 MPa, according to Satyanarayana et al. (2007). Therefore, this significant difference in ultimate tensile strength distribution can be attributed to defects of the residual fiber structure and surface, probably because these fibers are wastes generated during the manufacturing of useful fibers that are used in the industry.

Fig. 13b and c shows the frequency distribution of the ultimate tensile strength of the untreated and treated residual sisal fibers after the accelerated aging test by 72 h. Considering the range of tensile strength values found in this work, it was observed that the untreated fibers decreased the ultimate tensile strength distribution to lower than 70 MPa, but the values of the treated residual fibers were maintained between 150 MPa and 400 MPa.

Fig. 14a and b indicates the fiber break region after accelerated aging. As can be seen, untreated fibers present the fibrils peeled from the hemicellulose and lignin matrix, because of the degradation caused by the high alkalinity of the Brazilian ordinary cement Portland solution. This fact can be responsible for the low values of ultimate tensile strength. In contrast, treated fibers show the matrix preserved by the methane cold plasma treatment, helping to maintain the ultimate tensile strength of these fibers.

### 3.9. Pullout results

Fig. 15 shows the typical load-slip curves obtained in the pullout test. The results (Table 4) indicate that the treated fiber presents higher pullout load and shear stress. According to Ferreira et al. (2012) four regions are identified in the curve of the untreated fiber: the first (I) is the linear elastic region in which the adhesion is

**Table 4**
Results of pullout test of sisal fibers.

| $L$ (mm) | Treatment | $P_{max}$ (N) | $\tau_{max}$ (MPa) | $P_{Slip}$ (N) | $\tau_{Slip}$ (MPa) |
|---|---|---|---|---|---|
| 25 | Untreated | 3.73 (1.02) | 0.30 (0.08) | 2.56 (0.72) | 0.18 (0.04) |
| | Treated | 5.74 (0.77) | 0.44 (0.08) | 4.64 (0.72) | 0.33 (0.04) |

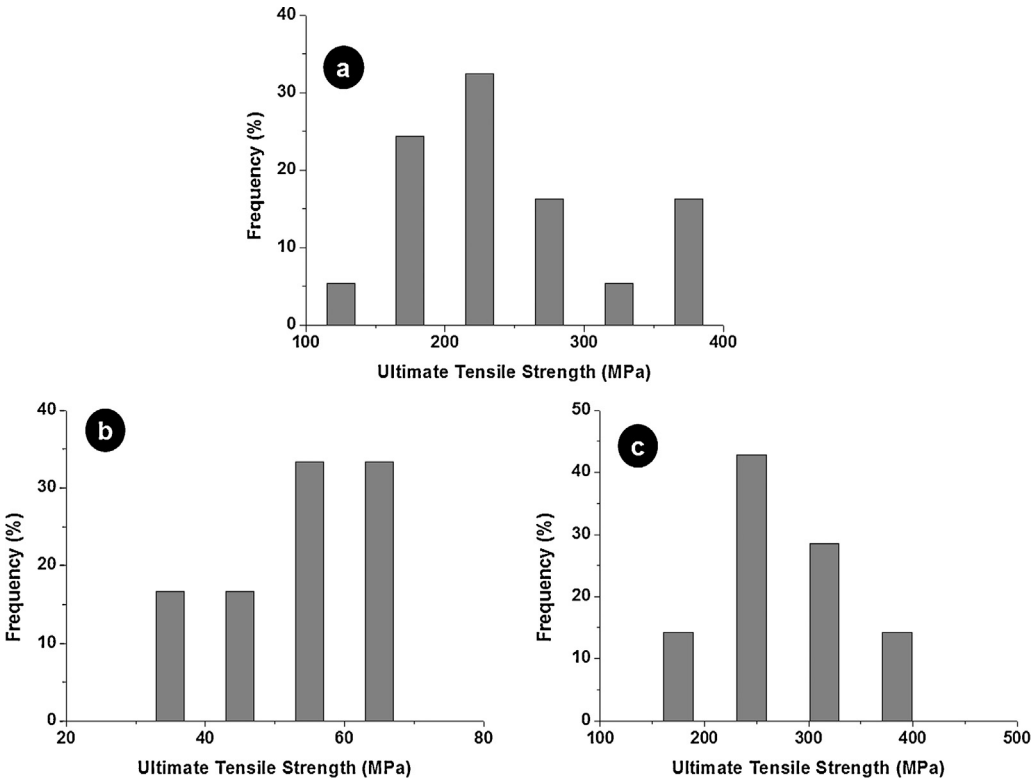


**Fig. 13.** Ultimate tensile strength frequency distribution of the residual sisal fibers. (a) Untreated residual sisal fiber before and (b) after accelerated aging, and (c) treated fiber after accelerated aging.

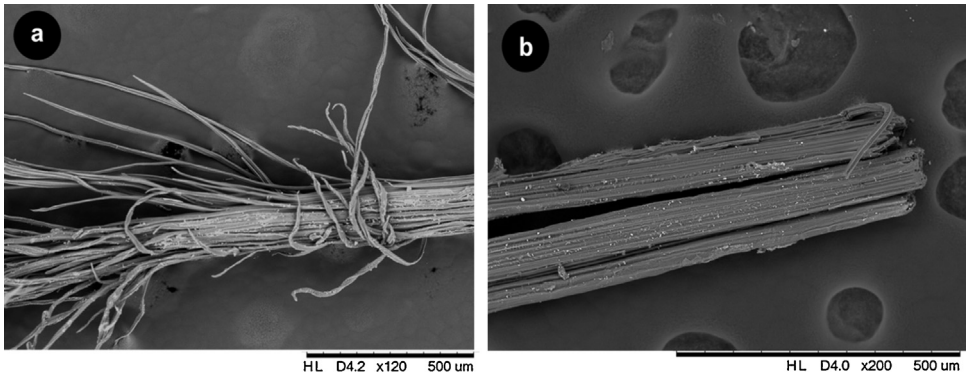


**Fig. 14.**

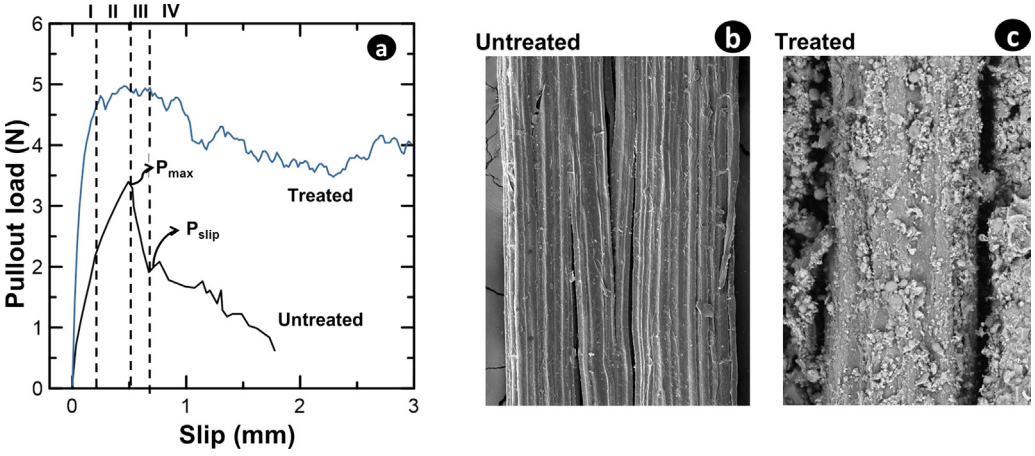


**Fig. 15.** (a) Typical curves of the pullout test of treated and untreated sisal fibers; fiber surface (b) untreated and (c) treated after pullout test.

considered perfect. In region II it can be observed the loss of linearity which is defined as the starting point of detachment between the fiber and matrix. This point is related to the interfacial detachment that propagates stably until the load reaches the peak, the highest pullout load ($P_{max}$). The region III, after the peak load, corresponds to the stage where the detachment is complete, or the fiber is entirely detached from the cement matrix. The region IV, indicated by $P_{slip}$, corresponds in fact to the slippage or debonding process of the fiber.

The results of the pullout tests indicated that plasma treatment promoted a degree of surface modification (Fig. 15b and c) and let the sisal fibers less subjected to the wet/dry shrinkage process; i.e. the treatment improved the interface between the fiber and brittle cement matrix without loss of adhesion by the oscillation of the cross section when fiber is submitted to wetting and drying cycles.

## 4. Implications

The fibers treated by methane cold plasma during 10 min presented a higher hydrophobicity when compared to untreated fibers. In addition, the treated fibers retained a good residual ultimate tensile strength distribution even after a severe accelerated aging test in saturated cement solution at 60 °C during 72 h. The results indicate clearly the potential of the methane cold plasma treatment to mitigate degradation of the fiber structure in cement matrix. These treated sisal fibers have a better adhesion on cement matrix and demonstrated that can be used for practical applications, including hybrid reinforcement in fiber-cement composites.

## 5. Conclusions

The cold methane plasma treatment induced significant superficial changes in the residual sisal fibers. The overall trend can be explained by the possible formation of an external polymerized layer on the surface, contributing to the increase of the dielectric constant and reducing the water absorption. From this experimental study, the following comments can be addressed:

- Untreated and treated surface sisal fibers were attacked by ions of the saturated cement Portland solution at 60 °C during three days. There was a significant difference between the surfaces observed regarding the calcium oxalate structures identified by SEM images.
- According to the X-ray diffraction patterns and FTIR measurements the bulk residual sisal fibers were not changed significantly by cold methane plasma treatment.
- The amount of absorbed water of the treated fibers is smaller than in the case of the corresponding untreated ones.
- The untreated fiber surface presented root mean square roughness, RMS, about 59 nm and treated fiber about 37 nm, according to SPM technique.
- The capacitance increased with increasing the water adsorption until the equilibrium for both types of fiber, but treated fibers presented a major dielectric constant of $3.1 \pm 0.3$ more than the double of the value corresponding to the untreated fibers.
- The methane cold plasma treatment increased the contact angle of the residual sisal fiber surface from $83^\circ \pm 13^\circ$ to $105^\circ \pm 4^\circ$.
- After accelerated aging test it was observed that the untreated fibers decreased the ultimate tensile strength distribution to lower than 70 MPa, but the values of the treated residual fibers were maintained between 150 MPa and 400 MPa.
- The fiber treated present the higher pullout load and shear stress than one untreated.

## Acknowledgments

The authors acknowledge the Brazilian financial support from Fundação de Amparo à Pesquisa do Estado de São Paulo (FAPESP, Grants nos.: 2008/04769-9, 2009/10614-0, 2009/17293-5; 2010/16524-0), Conselho Nacional de Desenvolvimento Científico e Tecnológico (CNPq, Grants nos.: 472133/2009-8, 305792/2009-1 and 310259/2010-0), Coordenação de Aperfeiçoamento de Pessoal de Nível Superior (CAPES, Projeto Pro Engenharias—PE 103/2008). The authors are gratefully acknowledged to Saulo R. Ferreira and Flávio A. Silva for their technical support to pullout tests in the Coppe—Instituto Alberto Luiz Coimbra de Pós-Graduação e Pesquisa de Engenharia.

## References

Alemdar, A., Sain, M., 2008. Isolation and characterization of nanofibers from agricultural residues—wheat straw and soy hulls. Bioresour. Technol. 99, 1664–1671.
Alvarez, V.A., Vázquez, A., 2006. Influence of fiber chemical modification procedure on the mechanical properties and water absorption of MaterBi-Y/sisal fiber composites. Compos. Part A: Appl. Sci. Manuf. 37, 1672–1680.
Anwer, Md. M., Bhuiyan, A.H., 2012. Influence of low temperature plasma treatment on the surface, optical and DC electrical properties of jute. J. Appl. Phys. 1, 16–22.
Bentur, A., Mindess, S., 2007. Fiber Reinforced Cementitious Composites, second ed. Elsevier Applied Science, London.
Bledzki, A.K., Gassan, J., 1999. Composites reinforced with cellulose based fibres. Prog. Polym. Sci. 24, 221–274.
Boerjan, W., Ralph, J., Baucher, M., 2003. Lignin biosynthesis. Rev. Plant Biol. 54, 519–546.
Bozaci, E., Sever, K., Sarikanat, M., Seki, Y., Demir, A., Ozdogan, E., Tavman, I., 2013. Effects of the atmospheric plasma treatments on surface and mechanical properties of flax fiber and adhesion between fiber-matrix for composite materials. Composites Part B 45, 565–572.
Carlsson, C.M.G., Ström, G., 1991. Reduction and oxidation of cellulose surfaces by means of cold plasma. Langmuir 7, 2492–2497.
Costa, T.H.C., Feitor, M.C., Alves Jr., C., Freire, P.B., Bezerra, C.M., 2006. Effects of gas composition during plasma modification of polyester fabrics. J. Mater. Process. Technol. 173, 40–43.
Felekoglu, B., Tosun, K., Baradan, B., 2009. A comparative study on the flexural performance of plasma treated polypropylene fiber reinforced cementitious composites. J. Mater. Process. Technol. 209, 5133–5144.
Ferreira, S.R., Lima, P.R.L., Silva, F.A., Toledo Filho, R.D., 2012. Effect of sisal fiber hornification on the adhesion with Portland cement matrices. Revista Matéria 17 (2), 1024–1034 (in Portuguese).
Franceschi, V.R., Nakata, P.A., 2005. Calcium oxalate in plants: formation and function. Annu. Rev. Plant Biol. 56, 41–71.
Friedrich, J., 2011. Mechanisms of plasma polymerization—reviewed from a chemical point of view. Plasma Process. Polym. 8, 783–802.
Fuentes, C.A., Tran, L.Q.N., Dupont-Gillain, C., Vanderlinden, W., De Feyter, S., Van Vuure, A.W., Verpoest, I., 2011. Wetting behavior and surface properties of technical bamboo fibres. Colloids Surf. A 380, 89–99.
Gaiolas, C., Costa, A.P., Nunes, M., Santos Silva, M.J., Belgacem, M.N., 2008. Grafting of paper by silane coupling agents using cold-plasma discharges. Plasma Process. Polym. 5, 444–452.
Gaiolas, C., Belgacem, M.N., Silva, L., Thielemanx, W., Costa, A.P., Nunes, M., Santos Silva, M.J., 2009. Green chemicals and process to graft cellulose fibers. J. Colloids Interface Sci. 330, 298–302.
Gandini, A., Belgacem, M.N., 2008. The state of the art. In: Belgacem, M.N., Gandini, A. (Eds.), Monomers, Polymers and Composites from Renewable Resources. Elsevier, pp. 1–16.
Ghorbanzadeh, A.M., Norouzi, S., Mohammadi, T., 2005. High energy efficiency in syngas and hydrocarbon production from dissociation of $CH_4$–$CO_2$ mixture in a non-equilibrium pulsed plasma. J. Phys. D: Appl. Phys. 38, 3804–3811.
Gutiérrez, R.M., Díaz, L.N., Delvasto, S., 2005. Effect of pozzolans on the performance of fiber-reinforced mortars. Cem. Concr. Compos. 27, 593–598.
Hua, Z.Q., Sitaru, R., Denes, F., Young, R.A., 1997. Mechanisms of oxygen- and argon-RF-plasma-induced surface chemistry of cellulose. Plasmas Polym. 2, 190–224.
Indarto, A., Choi, J.-W., Lee, H., Song, H.K., 2005. Kinetic modeling of plasma methane conversion using gliding arc. J. Nat. Gas Chem. 14, 13–21.
Kačuráková, M., Belton, P.S., Wilson, R.H., Hirsch, J., Ebringerová, A., 1998. Hydration properties of xylan-type structures: an FTIR study of xylooligosaccharides. J. Sci. Food Agric. 77, 38–44.
Kado, S., Kohei, U., Sekine, Y., Fujimoto, K., Nozaki, T., Okazaki, K., 2003. Reaction mechanism of methane activation using non-equilibrium pulsed discharge at room temperature. Fuel 82 (18), 2291–2297.
Kalia, S., Kaith, B.S., Kaur, I., 2011. Cellulose Fibers Bio- and Nano-Polymer Composites: Green Chemistry and technology. Springer, 737 p.

Kim, J.-H., Liu, G., Kim, S.H., 2006. Deposition of stable hydrophobic coatings with in-line CH4 atmospheric RF plasma. J. Mater. Chem. 16 (1), 977–981.
Kumar, V., Rauscher, H., Brétagnol, F., Arefi-Khonsari, F., Pulpytel, J., Colpo, P., Rossi, F., 2010. Preventing Biofilm Formation on Biomedical Surfaces. In: Rauscher, H., Perucca, M., Buyle, G. (Eds.), Plasma Technology for Hyperfunctional Surfaces: Food, Biomedical and Textile Applications. , first ed. Wiley-VCH Verlag GMbH & Co. KGaA, Weinheim, 428 p.
Li, Y., Mai, Y.W., Ye, L., 2000. Sisal fiber and its composites: a review of recent developments. Compos. Sci. Technol. 60 (11), 2037–2055.
Liu, Y.P., Hu, H., 2008. X-ray diffraction study of bamboo fibers treated with NaOH. Fiber Polym. 9 (6), 735–739.
Mahadeva, S.K., Yun, S., Kim, J., 2011. Flexible humidity and temperature sensor based on cellulose–polypyrrole nanocomposite. Sens. Actuators A 165 (2), 194–199.
Mahlberg, R., Niemi, H.E.M., Denes, F., Rowell, R.M., 1998. Effect of oxygen and hexamethyldisiloxane plasma on morphology, wettability and adhesion properties of polypropylene and lignocellulosics. Int. J. Adhes. Adhes. 18, 283–297.
Mármol, G., Santos, S.F., Savastano Jr, H., Borrachero, M.V., Monzó, J., Payá, J., 2013. Mechanical and physical performance of low alkalinity cementitious composites reinforced with recycled cellulosic fibres pulp from cement kraft bags. Ind. Crop. Prod. (in press).
Melo Filho, J.A., Silva, F.A., Toledo Filho, R.D., 2013. Degradation kinetics and aging mechanisms on sisal fiber cement composite systems. Cem. Concr. Compos. 40 (6), 30–39.
Morent, R., De Geyter, N., Verschuren, J., De Clerck, K., Kiekens, P., Leys, C., 2008. Non-thermal plasma treatment of textiles. Surf. Coat. Technol. 202 (14), 3427–3449.
Moniruzzaman, M., Ono, T., 2013. Separation and characterization of cellulose fibers from cypress wood treated with ionic liquid prior to laccase treatment. Bioresour. Technol. 127 (1), 132–137.
Motta, L.A.C., John, V., Agopyan, V., 2010. Thermo-mechanical treatment to improve properties of sisal fibres for composites. Mater. Sci. Forum 636–637, 235–259.
Nishiyama, Y., 2009. Structure and properties of the cellulose microfibril. J. Wood Sci. 55 (4), 241–249.
Navarro, F., Dávalos, F., González-C, R., López-Dellamary, F., Marínquez, R., Turrado, J., Ramos, J., 2009. Sisal chemo-thermomechanical pulp paper with a strongly hydrophobic surface coating produced by a pentafluorophenyldimethylsilane cold plasma. J. Appl. Polym. Sci. 112 (1), 479–488.
Novak, I., Elyashevich, G.K., Chodak, I., Olifirenko, A.S., Steviar, M., Spirkova, M., Saprykina, N., Vlasova, E., Kleinova, A., 2008. Polymer matrix of polyethylene porous films functionalized by electrical discharge plasma. Eur. Polym. J. 44 (8), 2702–2708.
Olaru, N., Olaru, L., Cobiliac, G.H., 2005. Plasma-modified wood fibers as fillers in polymeric materials. Rom. J. Phys. 50 (9–10), 1095–1101.
Ortiz, O., Castells, F., Sonnemann, G., 2009. Sustainability in the construction industry: a review of recent developments based on LCA. Constr. Build. Mater. 23 (1), 28–39.
Östenson, N., Järund, H., Toriz, G., Gatenholm, P., 2006. Determination of surface functional groups in lignocellulosic materials by chemical derivatization and ESCA analysis. Cellulose 13, 157–170.
Pacheco-Torgal, F., Jalali, S., 2011. Cementitious building materials reinforced with vegetable fibres: a review. Constr. Build. Mater. 25 (2), 575–581.
Pavasars, I., Hagberg, J., Borén, H., Allard, B., 2003. Alkaline degradation of cellulose: mechanisms and kinetics. J. Polym. Environ. 11 (2), 39–47.
Pereira, C.L., Savastano Jr, H., Payá, J., Santos, S.F., Borrachero, M.V., Monzó, J., Soriano, L., 2013. Use of highly reactive rice husk ash in the production of cement matrix reinforced with green coconut fiber. Ind. Crop. Prod. 49 (8), 88–96.
Pérez, S., Mazeau, K., 2005. Conformations, structures, and morphologies of celluloses. In: Dumitriu, S., Dekker, M. (Eds.), Polysaccharides: Structural Diversity and Functional Versatility. , second ed.
Popescu, C.-M., Tibirna, C.-M., Vasile, C., 2009. XPS characterization of naturally aged wood. Appl. Surf. Sci. 256 (15), 1355–1360.
Popescu, M.-C., Totolin, M., Tibirna, C.M., Sdrobis, A., Stevanovic, T., Vasile, C., 2011. Grafting of softwood kraft pulps fibers with fatty acids under cold plasma conditions. Int. J. Biol. Macromol. 48 (2), 326–335.
Ramakrishna, G., Sundararajan, T., 2005. Studies on the durability of natural fibres and the effect of corroded fibres on the strength of mortar. Cem. Concr. Compos. 27 (5), 575–582.
Rangel-Vázquez, N.A., Leal-García, T., 2010. Spectroscopy analysis of chemical modification of cellulose fibers. J. Mex. Chem. Soc. 54 (4), 192–197.
Sadova, S.F., Pankratova, E.V., 2009. Low-temperature plasma surface modification of textiles made from natural fibers and advanced technologies. High Energy Chem. 43 (3), 234–240.
Sahin, H.T., 2007. RF-CF4 plasma surface modification of paper: chemical evaluation of two sidedness with XPS/ATR-FTIR. Appl. Surf. Sci. 253 (9), 4367–4373.
Sain, M., 2000. X-ray photoelectron spectroscopy study of ultrathin-film-forming chemical-precursor-engineered lignocellulosic fiber and fiber-mat surfaces. Appl. Surf. Sci. 158 (1–2), 92–103.
Sain, M., Panthapulakkal, S., 2006. Bioprocess preparation of wheat straw fibers and their characterization. Ind. Crop. Prod. 23 (1), 1–8.
Satyanarayana, K.G., Guimarães, J.L., Wypych, F., 2007. Studies on lignocellulosic fibers of Brazil. Part I: source, production, morphology, properties and applications. Compos. Part A: Appl. Sci. Manuf. 38 (7), 1694–1709.
Savastano Jr., H., Santos, H.S.F., Radonjic, M., Soboyejo, W.O., 2009. Fracture and fatigue of natural fiber-reinforced cementitious composites. Cem. Concr. Compos. 31 (4), 232–239.
Savastano Jr., H., Warden, P.G., Coutts, R.S.P., 2005. Microstructure and mechanical properties of waste fiber–cement composites. Cem. Concr. Compos. 27 (5), 583–594.
Scrivener, K.L., Young, J.F., 1997. Mechanisms of Chemical Degradation of Cement-Based Systems, first ed. Spon Press, 455 p.
Shenton, M.J., Stevens, G.C., 2001. Surface modification of polymer surfaces: atmospheric plasma versus vacuum plasma treatments. J. Phys. D: Appl. Phys. 34 (18), 2761–2768.
Silva, F.A., Mobasher, B., Soranakom, C., Toledo Filho, R.D., 2011. Effect of fiber shape and morphology on interfacial bond and cracking behaviors of sisal fiber cement based composites. Cem. Concr. Compos. 33 (8), 814–823.
Sinha, E., Panigrahi, S., 2009. Effect of plasma treatment on structure, wettability of jute fiber and flexural strength of its composite. J. Comput. Matt. 43 (17), 1791–1802.
Siow, K.S., Britcher, L., Kumar, S., Griesser, H.J., 2006. Plasma methods for the generation of chemically reactive surfaces for biomolecule immobilization and cell colonization—a review. Plasma Process. Polym. 3 (6–7), 392–418.
Tan, T., Santos, S.F., Savastano Jr., H., Soboyejo, W.O., 2012. Fracture and resistance-curve behavior in hybrid natural fiber and polypropylene fiber reinforced composites. J. Mater. Sci. 47 (6), 2864–2874.
Taylor, H.F.W., 1997. Cement Chemistry, second ed. Thomas Telford Publishing.
Thomas, S., Paul, S.A., Pothan, L.A., Deepa, B., 2011. Natural fibres: structure, properties and applications. In: Kalia, S., Kaith, B.S., Kaur, I. (Eds.), Cellulose Fibers: Bio- and Nano-Polymer Composites. Green Chemistry Technology. Springer-Verlag, Berlin, pp. 3–44.
Tonoli, G.H.D., Rodrigues Filho, U.P., Savastano Jr, H., Bras, J., Belgacem, M.N., Rocco Lahr, F.A., 2009. Cellulose modified fibres in cement based composites. Composites Part: A 40, 2046–2053.
Tonoli, G.H.D., Belgacem, M.N., Siqueira, G., Bras, J., Savastano Jr., H., Rocco Lahr, F.A., 2013. Processing and dimensional changes of cement based composites reinforced with surface-treated cellulose fibres. Cem. Concr. Compos. 37, 68–75.
Tran, L.Q.N., Fuentes, C.A., Dupont-Gillain, C., Van Vuure, A.W., Verpoest, I., 2011. Wetting analysis and surface characterization of coir fibres used as reinforcement for composites. Colloids Surf. A 377 (1–3), 251–260.
Toledo Filho, R.D., Scrivener, K., England, G.L., Ghavami, K., 2000. Durability of alkali-sensitive sisal and coconut fibres in cement mortar composites. Cem. Concr. Compos. 22 (2), 127–143.
Tonoli, G.H.D., Savastano Jr., H., Santos, S.F., Dias, C.M.R., John, V.M., Rocco Lahr, F.A., 2011. Hybrid reinforcement of sisal and polypropylene fibers in cement-based composites. J. Mater. Civil Eng. 23 (2), 177–187.
Wielen, L.C.V., Ragauskas, A.J., 2004. Grafting of acrylamide onto cellulosic fibers via dielectric-barrier discharge. Eur. Polym. J. 40, 477–482.
Wielen, L.C.V., Elder, T., Ragauskas, A.J., 2005. Analysis of the topochemical effects of dielectric-barrier discharge on cellulosic fibers. Cellulose 12 (9), 185–196.
Wielen, L.C.V., Östenson, M., Gatenholm, P., Ragauskas, A.J., 2006. Surface modification of cellulosic fibers using dielectric-barrier discharge. Carbohydr. Polym. 65 (2), 179–184.
Xu, F., 2010. Structure, ultrastructure, and chemical composition. In: Sun, R.-C. (Ed.), Cereal Straw as a Resource for Sustainable Biomaterials and Biofuels: Chemistry, Extractives, Lignins, Hemicelluloses and Cellulose. Elsevier, Amsterdam, pp. 9–47.

## Further reading

Oladele, I.O., Akinwekomi, A.D., Aribo, S., Aladenika, A.K., 2009. Development of fiber reinforced cementitious composite for ceiling application. J. Miner. Mater. Charact. Eng. 8 (8), 583–590.

Spinacé, M.A.S., Lambert, C.S., Fermoselli, K.K.G., De Paoli, M.A., 2009. Characterization of lignocellulosic curaua fibres. Carbohydr. Polym. 77 (1), 47–53.

Vaswani, S., Koskinen, J., Hess, D.W., 2005. Surface modification of paper and cellulose by plasma-assisted deposition of fluorocarbon films, Surf. Coat. Technol. 195, 121–129.

Wolf, R., Sparavigna, A.C., 2010. Role of plasma surface treatments on wetting and adhesion. Engineering 6 (2), 397–402.

Żenkiewicz, M., 2007. Methods for the calculation of surface free energy of solids, J. Achiev. Mater. Manuf. Eng. 24 (1), 137–145.